TECHNISCHE MECHANIK
an open access journal

journal homepage: www.ovgu.de/techmech

Tech. Mech., Vol. 45, Is. 1, (2025), 110–125

Received: 18.07.2025
Accepted: 27.10.2025
Available online: 27.10.2025

A Corrosion Correction for Minimal Weight Design of Truss Structures under Compliance Constraint

Anton Tkachuk[1]*, and Mykola Tkachuk[2],

[1] Karlstad University, Department of Engineering and Physics, SE-658 88 Karlstad, Sweden
[2] National Technical University "Kharkiv Polytechnic Institute", 2, Kyrpychova Street, Kharkiv, 61002, Ukraine

Abstract: Corrosion-induced stiffness and strength reduction are often neglected in truss optimization. In the case of uniform corrosion of truss members, the stiffness reduction is proportional to the corroded area, and it has a significant effect during the typically required lifespan of steel truss structures. The corroded area can be predicted via a simplified model that takes into account the orientation of surfaces and the exposure time. The corrosion correction can be incorporated into minimal weight design under the global compliance constraint. The compliance constraint is formulated as a linear matrix inequality for a single load or multiple loads with an ellipsoidal uncertainty (a worst-case scenario problem). Herein, one continuous design variable is used to describe the area for rectangular cross-sections. The formulations with fixed width and with fixed aspect ratio yield convex and difference-of-convex programming problems, respectively. These problems are solved using interior-point methods with the CVX package* for disciplined convex programming called from MATLAB. The procedure scales well up to 1900 degrees of freedom and 3660 members on a laptop (producing a design within 8 minutes). The relative correction of the total mass of the structure due to corrosion is documented for illustrative examples. It can be larger than the loss area of the effective cross-section (typically 5-10%) under a specific condition.

Keywords: Truss structures, Corrosion effect, Minimum weight design, Semi-definite programming, Compliance constraint, Convex-concave procedure.

1 Introduction

Sizing of truss structures under volume, strength, compliance, eigenfrequency, or buckling constraints is a well-studied problem. Multiple analytical solutions are known, e.g., for cantilever truss structures under a point load (Michell, 1904; Prager, 1977), a truss structure under bending load (Chan, 1960) or other boundary conditions (Shield, 1971). For many other cases, numerical methods are employed (Stolpe, 2016; Rajan, 1995; Fleury, 1979; Svanberg, 1981). This problem has drawn attention from different communities, including applied mathematics and structural engineering. Therefore, it is not possible to describe all aspects of available methods; see a review paper for more details (Lógó et al., 2020). Herein, two main aspects are summarized: numerical method development and influence of the real environmental conditions as loads or structural degradation.
Sizing of truss structures motivated the development and application of various numerical algorithms, which can be grouped by the used optimization method

- Gradient-based methods (Svanberg, 1981; Khot, 1985) are general and efficient, except when the optimizer gets stuck in a local minimum. They scale extremely well for large problems.
- Particle swarm (Gomes, 2011) and genetic algorithms (Rajan, 1995; Lingyun et al., 2005), which are mainly gradient-free, are relatively easy to implement. Most types of constrains and objectives are compatible with the methods. These approaches are numerically less efficient than the gradient-based approaches. An advantage is a higher robustness against local minima.
- Semi-definite programming (SDP) approaches (Ben-Tal and Nemirovski, 1997; Achtziger and Kočvara, 2007) are robust and fast convergent up to a moderate system size. Compliance, buckling and base eigenfrequency constraints fit well to the approach (Kočvara, 2002; Ohsaki et al., 1999). If topology and node positions are fixed then the problem is affine with respect to design parameters and can be treated well with available solvers. Recently, also larger systems could be treated with specialized algorithms Habibi et al. (2023). However, non-convex constraints such as equality/inequalities on the higher frequencies and limits on the local displacements pose a difficulty for the approach.
- Second-order cone programming formulations (Kanno, 2016; Kočvara and Outrata, 2017) are comparable in robustness with semi-definite programming (SDP) approaches, furthermore improve numerical efficiency for many cases.
- Mixed-integer programming provides a solution close to practice (Stolpe, 2016), as the sizing optimization with a discrete set of section dimensions is combined with topology optimization.

The first four approaches primarily work with continuous design variables. Among these methods, we focus on SDP approaches for their robustness and extensibility to uncertainty for loads or for node positions (Yonekura and Kanno, 2010; Hashimoto and Kanno,

*CVX is a name that does not abbreviate to a specific word or phrase.

* E-mail address: anton.tkachuk@kau.se
doi: 10.24352/UB.OVGU-2025-044

2015). The approach is also helpful in identifying infeasible combinations of constraints for design problems. The application of SDP for truss design remains an area of active research with a focus on scalability for large problem sizes and advanced constraints (Habibi et al., 2021; Ma et al., 2025; Habibi, 2024; Tkachuk and Tkachuk, 2024).

Including real environmental conditions and structural degradation in the sizing of truss structures is challenging. A few examples in the literature include effects of temperature (Keleş et al., 2024), corrosion degradation (Aydoğdu et al., 2023), ice accretion and wind loads (Tsavdaridis et al., 2020; Kowalski et al., 2023). The study related to corrosion effects (Aydoğdu et al., 2023) is applied to a roof steel structure and assumes a special indoor corrosion law. Optimization constraints include displacement, stress, and individual member buckling. The minimization algorithm is based on swarm intelligence, which is a gradient-free approach that requires a large number of forward analyses. Other contributions include potential structural degradation without a deterministic environmental cause and seek so-called fail-safe designs. Changes in the obtained design are observed if the maximum volume with reduced stiffness (Achtziger and Bendsøe, 1999) is included. Moreover, a significantly different topology of truss structures is obtained if a maximum number of eliminated members is considered (Kanno, 2017; Stolpe, 2019).

Many studies of atmospheric corrosion of truss structures are empirical and semi-empirical. They describe corrosion rate as a function of material, coating, internal stress and environmental conditions such as temperature, humidity and salinity, see an example in Kainuma et al. (2021). Also, natural and anthropogenic air pollutants, mainly sulphur dioxide (SO_2) and chlorides (Leygraf, 2000), can significantly accelerate corrosion. Corrosion rate has a high level of uncertainty. However, using information from weather history and real measurements on cite (temperature and corrosion current) can increase accuracy of the corrosion prediction (Rasoli et al., 2020). Corrosion leads to stiffness and strength reduction (Shu et al., 2020; Jordan, 2019), which is difficult to formalize, taking into consideration all factors and the unique climate conditions at the location of the structure. Especially, the reduction of the ultimate strength due to pitting corrosion is difficult to model as location and depth of pits are randomly distributed along the structure (Wang et al., 2018). Furthermore, the stress concentration close to pit increases the peak stress, which is critical for a failure analysis. Here, the effect of member orientation is prioritized over other dependencies (Vera et al., 2003; Santana et al., 2020; Rodríguez-Yáñez et al., 2023). Only a deterministic model for corrosion is used.

The relevant required lifespan of steel structures depend on their task and discussed at various national standards. These values are often indicative and can be adjusted individually based on environmental conditions, maintenance and time spans between repair activities. For example, welding plates of fresh material on chords and diagonals of corroded bridges significantly extends life span in a sustainable way (Pipinato, 2018). As corrosion can be viewed as monotonous process of capacity degradation (strength or stiffness), each repair can be viewed as partial reversion of the process (Landolfo et al., 2011). Figure 1 shows qualitatively the process of capacity degradation over the time. British rules indicate following required life spans in different categories (British Standards Institution, 2005, Table 2.1): Temporary structures – 10 years; replaceable structural parts (e.g., gantry girders, bearings) – 10–30 years; bridges, and major civil engineering structures – 100–120 years. The American AASHTO LRFD Bridge Design Specifications defines a 75-year design life for highway bridges (Azizinamini et al., 2014). Researches set different life spans in their case studies, e.g., a roof supporting structure for an industrial environment is designed for 16 years (Aydoğdu et al., 2023). Herein, repairs are not considered and the typical required lifespan is selected as 60 years, being an average.

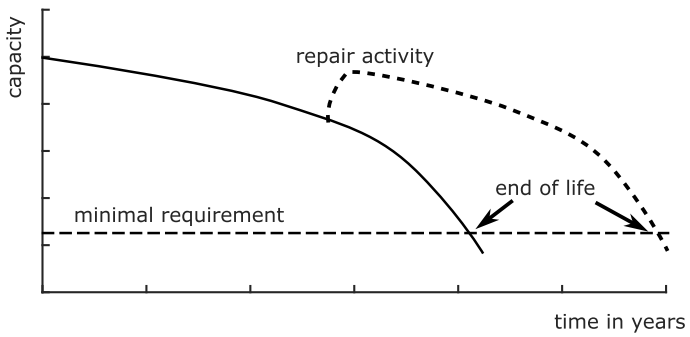

Fig. 1: Capacity degradation of a structure up to the end of life without and with intermediate repar activities.

The identified gap for the paper is to combine a more complex corrosion model than in Aydoğdu et al. (2023) with a different optimization strategy (SDP). The corrosion model does not include the effect of local corrosion (pitting) and corrosion in truss connections or supports (potential contact with ground or girder ends of steel bridges exposed to additional moisture Tzortzinis et al. (2021)). Corroded depth yields a simple model for stiffness correction for rectangular cross-sections. Only continuous variables for cross-sectional area are used as the design variables.. Optimization problems with a single load case and a worst-case scenario with an ellipsoidal uncertainty are considered. For simplicity and clarity, all loads are considered active or linearly dependent on the design variables, e.g., self-weight. Furthermore, the dual problem (minimum compliance for the given weight) is not considered here.

The paper is organized into five sections and one appendix. The corrosion model is described in Section 2. Section 3 introduces the proposed sizing procedure for 2D trusses, focusing on three problem statements with different assumption and their mathematical formulations. The numerical results for three optimization cases are presented in Section 4. Conclusions are given in Section 5. Appendix A.1 discusses the limitation of the proposed formulation to square hollow sections.

2 Corrosion model

Consider a rectangular cross-section with the initial dimensions $w \times h$ as shown in Figure 2. The fixed width (FW) and the fixed aspect ratio (FAR) cases are considered below. Due to corrosion, the effective cross-section reduces to the dimensions $w_r \times h_r$. Exposure angle and face orientation influence the rate of corrosion. Herein, the average corrosion rate v_r for groundward and skyward direction is assumed to follow the linear law with respect to the angle of exposure ϕ with respect to the horisontal orientation as suggested in Rodríguez-Yáñez et al. (2023)

$$v_r(\phi) = a\phi + b, \tag{1}$$

where a and b are constants, depending on climate, the position of the structure and the material. For the side faces, the average corrosion rate is assumed (1) for $\phi = 90°$. Vertical faces in the considered experiment correspond to this angle. This orientation enables water freely flow down and reduce the corrosion rate. The measured values of a are negative.. Thus, the reduction of the cross-sectional dimensions for the required lifespan of the structure t

$$w - w_r = (a \times 90° + b)t = v_r(90°)t, \tag{2}$$

$$h - h_r = (a\phi + b)t = v_r(\phi)t. \tag{3}$$

is linear in time t; however, other time dependencies are presented in the literature (Knotkova-Cermakova et al., 1982). The effective cross-section for stiffness calculation is expressed via the original cross-sectional area and time

$$A_r = w_r h_r = (w - v_r(90°)t)(h - v_r(\phi)t) = wh - t\left(hv_r(90°) + wv_r(\phi)\right) + v_r(\phi)v_r(90°)t^2. \tag{4}$$

For simplicity of the expression, only cases with fixed width or fixed aspect ratio are considered below, even though these cases may seem academic. If we fix the width of the cross-section w and use the height h as the design variable then the expression in (4) is affine of height h. This expression can be recast

$$A_r = wh - c_1 h + c_0, \tag{5}$$

where two constants are denoted with $c_1 = v_r(90°)t$ and $c_0 = v_r(\phi)v_r(90°)t^2 - wv_r(\phi)t$.

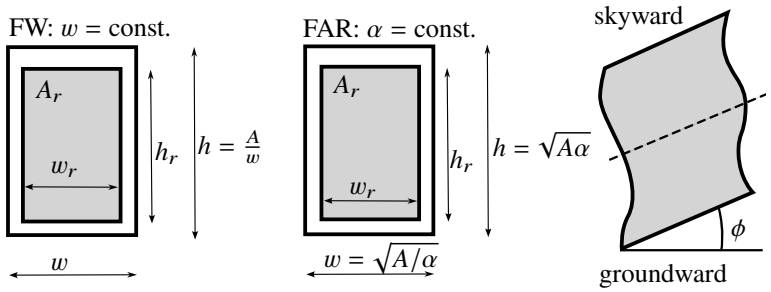

Fig. 2: Reduction of the cross-section due to corrosion for the cases with fixed width (left) and fixed aspect ratio (middle) and the definition of the inclination angle (right).

The case of fixed aspect ratio is treated differently, as A_r is a good candidate for the design variable. The original area and the efficient area are related

$$A_r = w_r h_r = (w - v_r(90°)t)(h - v_r(\phi)t) = \left(\sqrt{\frac{A}{\alpha}} - v_r(90°)t\right)\left(\sqrt{\alpha A} - v_r(\phi)t\right) = A - d_{0.5}\sqrt{A} + d_0, \tag{6}$$

where $\alpha = h/w$ is the aspect ratio and two constants are denoted with $d_{0.5} = t\left(v_r(90°)\sqrt{\alpha} + \frac{v_r(\phi)}{\sqrt{\alpha}}\right)$ and $d_0 = v_r(\phi)v_r(90°)t^2$. Solving the latter for the initial area A gives a real positive root

$$A = A_r - d_0 + \frac{d_{0.5}^2}{2} + \frac{d_{0.5}}{2}\sqrt{4A_r - 4d_0 + d_{0.5}^2}. \tag{7}$$

A Taylor expansion of (7) around $t = 0$ up to t^2 yields an approximate expression

$$A \approx A_r - d_0 + \frac{d_{0.5}^2}{2} + d_{0.5}\sqrt{A_r}. \tag{8}$$

The difference between (7) and (8) stays small for reasonable cross-sectional areas and required life as illustrated in Figure 3. Such an approximate expression can be useful in further studies, where an exact expression similar to eq. (7) is unavailable. An example of such a relation is given in Appendix with eq. (A.3).
Relations (7) and (8) have a dominant linear (convex) term A_r and a minor square root term depending on A_r. Both minor terms are concave and can be treated in a special way.

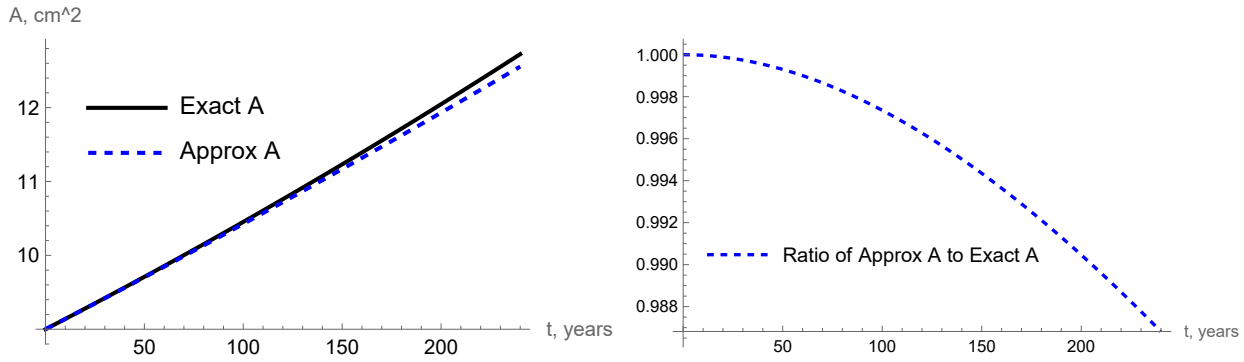

Fig. 3: Comparison of the initial area A from (7) and (8) (left) as a function of time for effective area $A_r = 9$ cm^2, aspect ratio $\alpha = 3$ and corrosion parameters $a = -0.120 \cdot 10^{-4}$ cm/year/$^\circ$ and $b = 20.0 \cdot 10^{-4}$ cm/year from Rodríguez-Yáñez et al. (2023). The ratio between both expressions is shown right.

3 Sizing procedure

3.1 Problem statement with a corrosion correction

To formulate the problem concisely, we introduce several quantities: the global stiffness matrix, the compliance, and the total mass of the structure as built. Herein, the description is restricted to pin-joint truss structure with straight members. Therefore, linear 2-node truss elements (of order one or $p = 1$) are used. The global stiffness matrix of the truss structure $\mathbf{K}$ is built from the local stiffness matrices $\mathbf{K}_e$ including the reduction of the effective cross-sectional area with

$$\mathbf{K} = \sum_{e=1}^{N} \mathbf{K}_e, \tag{9}$$

$$\mathbf{K}_e = \mathbf{B}_e^{\mathrm{T}} (E A_r L_e) \mathbf{B}_e, \tag{10}$$

$$\mathbf{B}_e = \frac{1}{L_e} \left[-\cos(\phi_e) \quad -\sin(\phi_e) \quad \cos(\phi_e) \quad \sin(\phi_e) \right], \tag{11}$$

where N is the total number of members, E is Young's modulus, L_e is the length of e^{th} truss and ϕ_e is the orientation angle of element e. The strain-displacement operator is denoted with $\mathbf{B}_e$.

The heights of individual members h_e and the effective cross-sectional area A_{re} are used as the design variable for FW and FAR cases, respectively. These continuous design variables are collected in a vector $\mathbf{s} \in \mathcal{R}^N$.

Application of boundary conditions lead to the reduced stiffness matrix $\tilde{\mathbf{K}}(\mathbf{s}) \in \mathcal{R}^{p \times p}$, where p is the number of free degrees of freedom. With respect to the reduced stiffness matrix and a single load vector $\mathbf{f} \in \mathcal{R}^p$, the displacement vector can be computed as

$$\mathbf{u} = \left(\tilde{\mathbf{K}}(\mathbf{s}) \right)^{-1} \mathbf{f}. \tag{12}$$

The global compliance is defined as

$$\tau = \mathbf{f}^{\mathrm{T}} \mathbf{u} = \mathbf{f}^{\mathrm{T}} \left(\tilde{\mathbf{K}}(\mathbf{s}) \right)^{-1} \mathbf{f}. \tag{13}$$

This expression for compliance is used later for a global displacement constraint. It is known to be convex w.r.t. cross-sectional areas of elements. Any local displacement constraints are omitted due to their non-convex nature. The force vector can also depend on the design parameters, as in the case of self-weight. These nodal forces are added to the active forces. For the sake of clarity, the dependence is excluded in the equations below.

In the case of ellipsoidal uncertainty of the load, the definition of compliance is less straightforward (Kanno, 2011, Proposition 3.1.5). Consider k vectors for load $\mathbf{F} = (\mathbf{f}_1, \mathbf{f}_2, \cdots, \mathbf{f}_k)$, which combine in the worst-case scenario by uncertain parameters $\boldsymbol{\zeta}$ within a unit sphere in $\mathcal{R}^k$

$$\mathcal{F} = \{ \mathbf{F}\boldsymbol{\zeta}, |\boldsymbol{\zeta}| \leq 1 \}. \tag{14}$$

There exists an infinite number of potential load scenarios, but the compliance should not exceed the given upper bound for any of them. We limit the analysis of load uncertainty to the case of fixed width rectangular cross-sections. A combination of a fixed aspect ratio cross-section configuration with uncertain load is possible. There are other formulations describing independent uncertainties in the direction or amplitude of point loads at nodes of trusses (Balogh et al., 2018; Csébfalvi and Lógó, 2020), but it is not considered herein.

Finally, the total mass of the structure as built is a natural objective. The total mass is expressed through the suggested design

variables for different cases of corrosion correction given in (5),(7),(8), respectively

$$W = \rho \sum_{e=1}^{N} L_e A_e = \rho \sum_{e=1}^{N} L_e w h_e = \rho w \sum_{e=1}^{N} L_e s_e, \tag{15}$$

$$W = \rho \sum_{e=1}^{N} L_e A_e = \rho \sum_{e=1}^{N} L_e \left(s_e - d_0 + \frac{d_{0.5}^2}{2} + \frac{d_{0.5}}{2} \sqrt{4 s_e - 4 d_0 + d_{0.5}^2} \right), \tag{16}$$

$$W = \rho \sum_{e=1}^{N} L_e A_e = \rho \sum_{e=1}^{N} L_e (s_e - d_0 + d_{0.5}^2 + d_{0.5} \sqrt{s_e}). \tag{17}$$

Three problem statements are solved in the paper with a primary focus on easiness of formulation.

FW. Given the topology of a truss structure with rectangular cross-sections and fixed nodal positions. The width of all members is fixed to be w and the height can vary within the limits $\underline{h} \le h_e \le \bar{h}$. A linear model for corrosion is assumed to be valid (1) and the required lifespan t is given. Furthermore, maximum compliance of the corroded structure $\bar{\tau}$ is given for a load vector $\mathbf{f}$. Find the design variables h_e that minimize the weight and satisfy the limits on height and compliance constraints.

FAR. Given the topology of a truss structure with rectangular cross-sections and fixed nodal positions. The aspect ratio for all cross sections is α. The area can vary within limits $\underline{A} \le A_e \le \bar{A}$. A linear model for corrosion is assumed to be valid (1) and the required lifespan t is given. Furthermore, maximum compliance of the corroded structure $\bar{\tau}$ is given for a load vector $\mathbf{f}$. Find design variables A_e that minimize the weight and satisfy the limits on height and compliance constraints.

Fixed width with uncertain load (FWUL). Given the topology of a truss structure with rectangular cross-sections and fixed nodal positions. The width of all members is fixed to be w and the height can vary within the limits $\underline{h} \le h_e \le \bar{h}$. A linear model for corrosion is assumed to be valid (1) and the required lifespan t is given. Furthermore, maximum compliance of the corroded structure $\bar{\tau}$ is given for k load vectors $\mathbf{f}_k$ with ellipsoidal uncertainty. Find design variables h_e that minimize the weight and satisfy the limits on height and compliance constraints.

FW and FWUL limits on the height in form $\underline{h} \le h_e \le \bar{h}$ directly constraints the cross-sectional area $w\underline{h} \le A_e \le w\bar{h}$. The limits on the area are more common in the literature and for the fixed w can be transferred to considered examples.

3.2 Formulations via semi-definite programming

The important ingredient of the formulation is the compliance constraint. Recasting (13) in an inequality yields

$$\bar{\tau} - \mathbf{f}^{\mathrm{T}} \left(\tilde{\mathbf{K}}(\mathbf{s}) \right)^{-1} \mathbf{f} \ge 0. \tag{18}$$

Herein, it is enforced according to Achtziger and Kočvara (2007) or (Kanno, 2011, Sec. 3.1.1) using a standard trick with Schur complement as a linear matrix inequality (LMI)

$$\begin{bmatrix} \tau & \mathbf{f}^T \\ \mathbf{f} & \tilde{\mathbf{K}}(\mathbf{s}) \end{bmatrix} \succcurlyeq 0, \qquad \tau \le \bar{\tau} \tag{19}$$

with an auxiliary variable τ. The symbol $\succcurlyeq 0$ denotes that the matrix on the left hand side is semi-definite (in this case of size $\mathcal{R}^{(p+1)\times(p+1)}$).

The ellipsoidal uncertainty of the load defined in (14) is discussed in (Kanno, 2011, Sec. 3.1.3). The compliance constraint for this case reads

$$\begin{bmatrix} \tau \mathbf{I}_{k\times k} & \mathbf{F}^T \\ \mathbf{F} & \tilde{\mathbf{K}}(\mathbf{s}) \end{bmatrix} \succcurlyeq 0, \qquad \tau \le \bar{\tau}. \tag{20}$$

This linear matrix inequality has size $\mathcal{R}^{(p+k)\times(p+k)}$ and $\mathbf{I}_{k\times k}$ denotes an identity matrix of dimension k.

The considered three problem statements are now formulated as SDP.

FW. The optimal heights of the trusses $s_e = h_e$ are recovered from optimization problem for weight (15) with the compliance constraint (19).

$$\begin{aligned} (\mathbf{s}^*, \tau^*) = \arg\min_{\mathbf{s},\tau} \; & \rho w \sum_{e=1}^{N} L_e h_e \\ & \underline{h} \le h_e \le \bar{h} \\ & \begin{bmatrix} \tau & \mathbf{f}^T \\ \mathbf{f} & \tilde{\mathbf{K}}(\mathbf{s}) \end{bmatrix} \succcurlyeq 0 \\ & \tau \le \bar{\tau}. \end{aligned} \tag{21}$$

FAR. The optimal effective areas of the trusses $s_e = A_{re}$ are recovered from optimization problem for weight (17) with the

compliance constraint (19)

$$
\begin{aligned}
(\mathbf{s}^*, \tau^*) = \arg\min_{\mathbf{s},\tau} \rho \sum_{e=1}^{N} L_e \left(A_{re} + \sqrt{A_{re}} d_{0.5} + d_0 \right) \\
\underline{A}_{re} \leq A_{re} \leq \bar{A}_{re} \\
\begin{bmatrix} \tau & \mathbf{f}^T \\ \mathbf{f} & \tilde{\mathbf{K}}(\mathbf{s}) \end{bmatrix} \succcurlyeq 0 \\
\tau \leq \bar{\tau}.
\end{aligned}
\tag{22}
$$

The objective is the difference-of-convex function, and the solution is found by a convex-concave procedure (Magnanti and Stratila, 2012; Lipp and Boyd, 2016). The square root term in the weight objective (17) is the concave part of the objective. It is linearised around the last found solution. Thus, the solution is iteratively found in a series of modified SDP problems

$$
\begin{aligned}
(\mathbf{s}^{*,(j+1)}, \tau) = \arg\min_{\mathbf{s},\tau} \rho \sum_{e=1}^{N} L_e \Delta_e^{(j)} A_{re} \\
\underline{A}_{re} \leq A_{re} \leq \bar{A}_{re} \\
\begin{bmatrix} \tau & \mathbf{f}^T \\ \mathbf{f} & \tilde{\mathbf{K}}(\mathbf{s}) \end{bmatrix} \succcurlyeq 0 \\
\tau \leq \bar{\tau},
\end{aligned}
\tag{23}
$$

$$
\Delta_e^{(j)} = 1 + \frac{d_{0.5}}{2\sqrt{A_{re}^{(j)}}},
\tag{24}
$$

where $\Delta_e^{(j)}$ is weighting[1]. Herein, the separable nature of the objective (23) is not completely used and more efficient methods are possible in future. In the case of the weight objective (16), the procedure is the same as for statement (23) and (24). The weighting changes to

$$
\Delta_e^{(j)} = 1 + \frac{d_{0.5}}{\sqrt{4A_{re}^{(j)} - 4d_0 + d_{0.5}^2}}.
\tag{25}
$$

FWUL. The optimal heights of the trusses $s_e = h_e$ are recovered from the optimization problem for weight (15) with the compliance constraint (20).

$$
\begin{aligned}
(\mathbf{s}^*, \tau^*) = \arg\min_{\mathbf{s},\tau} \rho w \sum_{e=1}^{N} L_e h_e \\
\underline{h} \leq h_e \leq \bar{h} \\
\begin{bmatrix} \tau \mathbf{I}_{k\times k} & \mathbf{F}^T \\ \mathbf{F} & \tilde{\mathbf{K}}(\mathbf{s}) \end{bmatrix} \succcurlyeq 0 \\
\tau \leq \bar{\tau}.
\end{aligned}
\tag{26}
$$

3.3 Implementation details, objective and constraint scaling

The algorithms are prototyped in MATLAB relying on the open-source package for disciplined convex optimization CVX (Grant and Boyd, 2008). The main advantages are effective code writing and easy access to interior-point method solvers for SDP such as SDPT3, SeDuMi or MOSEK [2]. Furthermore, the problem is automatically checked by CVX with respect to the strict rules of convex optimization. A disadvantage is the overhead for interpretation of CVX expression into problem structures used in the external solvers.

Performance of the interior-point method improves with a proper scaling of the constraints and variables as suggested in (Grant and Boyd, 2020, Sec. 10.4) and (MOSEK ApS, 2022, Sec. 7.3). This scaling affects the conditioning of the solved linear systems, improving numerical stability.

[1] Similar re-weighting procedure is also known for rank minimization of semi-definite matrix using log-det heuristic, where the weighting in the matrix trace objective is updated each iteration (Fazel et al., 2003)

[2] Herein, a combination MATLAB version: (R2024a) and CVX version 2.2 (Grant and Boyd, 2020) on win10 with SDPT3 version 4.0 (Tütüncü et al., 2003), SeDuMi version 1.3.4 (Sturm, 1999) or MOSEK version 10.2.1 (MOSEK ApS, 2022) is used. Double precision is used for all computations. High precision setting for optimizer are set in CVX. Maximum of 80 interior point iterations is set for all examples.

The weight objective is scaled by a reference value defined for fixed width and fixed aspect ratio cases with

$$M_{ref} = \rho w \sum_{e=1}^{N} L_e \underline{h}_e, \tag{27}$$

$$M_{ref} = \rho \sum_{e=1}^{N} L_e \underline{A}_{re}, \tag{28}$$

$$W_{scaled} = \frac{W}{M_{ref}}. \tag{29}$$

The reference value for stiffness $K_{\max} = 0.1 \max_{1\le i,j\le n} |K_{ij}(\tilde{\mathbf{s}})|$ is used in compliance constraint, similar to (Tkachuk and Tkachuk, 2024). The modified compliance reads as follows

$$\begin{bmatrix} \tau & \frac{\mathbf{f}^T}{\sqrt{K_{\max}}} \\ \frac{\mathbf{f}}{\sqrt{K_{\max}}} & \frac{\mathbf{K}(\mathbf{s})}{K_{\max}} \end{bmatrix} \succcurlyeq 0. \tag{30}$$

Further implementation detail concerns calculation of the limits effective areas $\underline{A}_{re}$ and $\bar{A}_{re}$ in (23) while the limits in the problem statement are given for the initial areas $\underline{A}_e$ and $\bar{A}_e$. Using the definition of the aspect ratio and depth of the corroded material,

$$\underline{A}_{re} = \left(\sqrt{\frac{\underline{A}_e}{\alpha}} - v_r(90°)t\right)\left(\sqrt{\alpha \underline{A}_e} - v_r(\phi)t\right) = \underline{A}_e - d_{0.5}\sqrt{\underline{A}_e} - d_0 + d_{0.5}^2, \tag{31}$$

$$\bar{A}_{re} = \left(\sqrt{\frac{\bar{A}_e}{\alpha}} - v_r(90°)t\right)\left(\sqrt{\alpha \bar{A}_e} - v_r(\phi)t\right) = \bar{A}_e - d_{0.5}\sqrt{\bar{A}_e} - d_0 + d_{0.5}^2. \tag{32}$$

The iterative convex-concave procedure is solved iteratively and it is often suggested to stop the process after the increment of the design variables falls below the specified threshold (Lipp and Boyd, 2016). Herein, a fixed number of iterations is used with default value $n_{\text{iter}} = 7$.

3.4 An illustrative two-member example with fixed width rectangular sections and one load case

This example has a closed-form solution and illustrates a specific condition for the total mass correction. Consider two consecutive horizontal trusses with equal width $w = 1$ and elasticity modulus E shown in Figure 4. Extreme nodes are fixed and the middle node is loaded by force F. Truss 1 provides a more efficient load path compared to truss 2 because it is four times shorter. Truss 2 provides a redundant load path. The height of the trusses is in the range $1 \le h_e \le 2$. Due to corrosion, the height of each truss is reduced by $h - h_r = tv_r(0°) = 0.1$ and the width is not reduced at all $w - w_r = tv_r(90°) = 0$. Optimal designs are compared at two levels of load: low load with a dimensionless compliance $T_{\text{low}} = \frac{F^2}{Ew\bar{\tau}} = \frac{1}{7}$ and high load $T_{\text{high}} = \frac{F^2}{Ew\bar{\tau}} = \frac{10}{43}$. The compliance constraints for single degree system with and without corrosion read

$$T - \frac{h_1}{10} - \frac{h_2}{40} \le 0, \tag{33}$$

$$T - \frac{h_1 - 0.1}{10} - \frac{h_2 - 0.1}{40} \le 0. \tag{34}$$

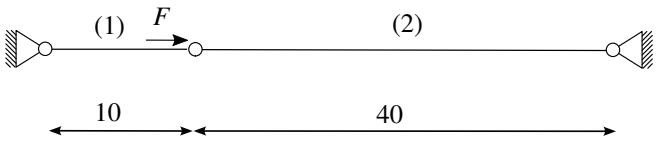

Fig. 4: Setup for an illustrative example (dimensionless example).

The volume objective $V_i^* = 10h_1^* + 40h_2^*$ for the optimal designs for each of four cases is presented in Table 1. The last column of the table gives β, which denotes the relative correction of the volume for the optimal design due to corrosion. It is 2.41 % and 27.74 % for low and high levels of load, respectively. At the high load, the height of the truss 1 is at the upper limit. The deficit in the compliance can only be compensated by increasing h_2, i.e., using the less efficient load path. The contribution of truss 2 to the compliance is 16 times less efficient for a unit added volume. Thus, the relative correction for the volume or mass can be greater than the area loss of the effective cross-section (5% for the height $h = 2$). For the low load level, the correction is comparable to the loss of the effective cross-section. This feature is observed in the following numerical examples.

Tab. 1: Optimal designs for the illustrative example

Case	Load level	Corrosion	h_1^*	h_2^*	V^*	β, %
1	low	no	1.17857	1.0	51.7857	-
2	low	yes	1.30357	1.0	53.0357	2.41
3	high	no	2.0	1.30233	72.093	-
4	high	yes	2.0	1.80233	92.093	27.74

4 Results for minimal weight design with corrosion correction

Next three numerical examples illustrate the performance of the proposed sizing procedure with the corrosion correction. The standard model for corrosion of carbon steels is selected from (Rodríguez-Yáñez et al., 2023) and the standard required life is chosen $t = 60$ years. These corrosion parameters are in the range of corrosivity category C5 (severe) for the international standard ISO 9223:2012. The dimensions of the examples increase from 17 to 3660 trusses and it is limited by the scaling of SDP solvers. We primarily report the required increase of the total mass m_{corr} or relative increase $\beta = m_{\text{corr}}/m_{\text{ref}}$ to satisfy the compliance constraint compared to the solution without corrosion. The relative increase β is in the range of 4% to 17% for the standard required life for the considered examples. Furthermore, the accumulated number of iterations and CPU time are reported where it is appropriate.

4.1 Example 1: 17-member truss

A 2D truss structure with 17 members is loaded on the tip with a force $F = 500$ kN and fixed at both nodes at the root, see Figure 5. The maximum admissible vertical displacement at the tip after required life $t = 60$ years is $\bar{v}_{\text{tip}} = 4$ cm, which corresponds to maximum admissible compliance $\bar{\tau} = 20$ kN·m. Six cases of problem setting are given in Table 2. All cases use the same elasticity $E = 206.8$ GPa and density $\rho = 7418$ kg/m^3, but they have different corrosion rates, parametrizations of the cross-section and optional self-weight. Case 1 is the fixed width with the standard corrosion parameters. Case 2 is a fixed width design that neglects member orientation influence on the corrosion rate ($a = 0$). Case 3 and 4 consider fixed aspect ratio problems with the standard corrosion parameters with different lower bounds on area. Upper limit on the cross-sectional area are the same for all cases (100 cm^2). The lower limit on the cross-sectional area are the same in cases 1-3 (25 cm^2). Case 4 has reduced lower limit on the cross-sectional area to 9 cm^2. Cases 5 and 6 include self-weight of the structure using $g = 9.81$ m/s^2 being otherwise identical to cases 0 and 1.

Tab. 2: Parameters for the design problem in Example 1.

Case	Attr.	a, cm/year/°	b cm/year	w, cm	$\bar{h}$, cm	$\underline{h}$, cm	α	$\bar{A}$, cm^2	$\underline{A}$, cm^2	self-weight
0	FW	0	0	5	20	5	-	-	-	off
1	FW	$-0.120 \cdot 10^{-4}$	$20.0 \cdot 10^{-4}$	5	20	5	-	-	-	off
2	FW	0	$20.0 \cdot 10^{-4}$	5	20	5	-	-	-	off
3	FAR	$-0.120 \cdot 10^{-4}$	$20.0 \cdot 10^{-4}$	-	-	-	1	25	100	off
4	FAR	$-0.120 \cdot 10^{-4}$	$20.0 \cdot 10^{-4}$	-	-	-	1	9	100	off
5	FW	0	0	5	20	5	-	-	-	on
6	FW	$-0.120 \cdot 10^{-4}$	$20.0 \cdot 10^{-4}$	5	20	5	-	-	-	on

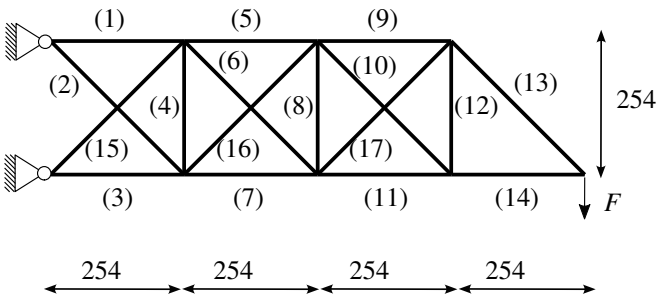

Fig. 5: Setup of Example 1. All sizes are in cm.

The following general observations can be made about the designs obtained in Figure 6 and Table 3. The trusses in upper and lower belts (members 1, 3, 5 and 7 for all cases) have the upper limit for cross-section areas as they provide the most efficient contribution to compliance. A few bracing trusses (members 4, 8, 10 and 12) have the lowest limit of the cross-section as they contribute less. The summary about the total weight increase and required number of iterations is given in Table 4. In case 1 (the standard corrosion model), a moderate weight increase by 4.9% is observed due to corrosion correction. In case 2, the corrosion correction is higher compared to case 1 (9.1 % vs. 4.9 %) as the model predicts higher cross-section reduction for trusses with

vertical and 45° orientation, see the optimal values of area for trusses 2, 6, 13 15 and 16. In case 3, the corrosion correction is slightly higher compared to case 1, even though the perimeter of a square section is less than the fixed width sections of the same area. The used corrosion model predicts a lower corrosion rate for vertical (side) surfaces making the fixed width design more efficient. In case 4, the design is more efficient compared to case 1, as the inefficient members (4, 8, 10 and 12) reduce their cross-sections from 25 to 9 cm^2. Addition of the self-weight yields similar designs to the counterparts without self-weight: Case 5 compared to Case 0 adds 3.4% of the total mass (mainly in members 2, 6, 9, 11 and 13), Case 6 against 1 – 8.3%. The proposed algorithm requires a similar number of iterations to converge (17). The masses of structure for cases 5 and 6 are 1938.0 kg and 2135.7 kg, respectively (β = 10.9%, mainly in members 2, 6, 9, 11, 13, 14 and 15). Thus, these cases illustrate the operation of the algorithm with self-weight, fixed-width and single load case.

The effect of parameter a in the corrosion model can be observed on degradation rates for the compliance between cases 1 and 2, shown in Figure 8. The negative value of a reduces the corrosion rate for trusses with vertical and 45° orientations, which also reduces the degradation rate for the compliance. The compliances for both cases reach the upper limit value of $\bar{\tau}$ = 20 kN·m at the required life span of 60 years. Noteworthy, the compliance is reciprocal to stiffness and it grows monotonically over time. A contrary qualitative behavior is shown in Figure 1 where the capacity (stiffness) reduces over time.

All the designs are obtained within a second on a laptop. SeDuMi and SDPT3 use 17 and 18 interior point iterations with high accuracy settings[3], respectively. Seven convex-concave iterations are enough to converge in the fixed aspect ratio case. The proposed scaling scheme gives an improvement for convergence at higher iterations, see Figure 7.

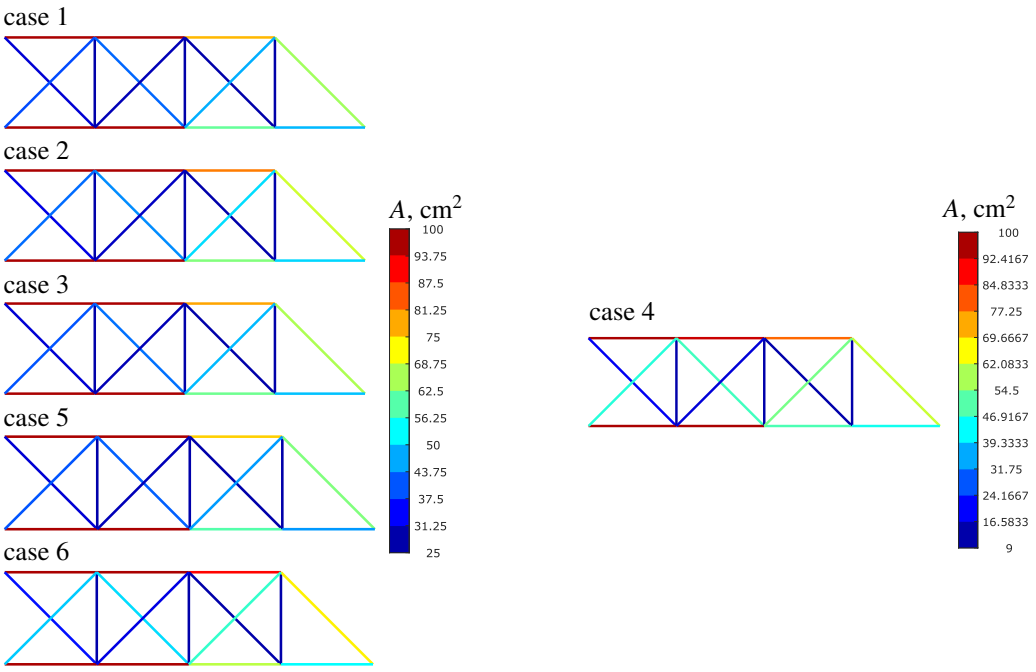

Fig. 6: Visualization of cross-sectional areas for Example 1.

Tab. 3: Obtained designs for Example 1 given as the cross-sectional area in cm^2.

	Member																
case	1	2	3	4	5	6	7	8	9	10	11	12	13	14	15	16	17
0	100.0	26.7	100.0	25.0	100.0	35.8	100.0	25.0	71.7	25.0	56.9	25.0	60.6	42.9	34.0	25.0	40.8
1	100.0	28.6	100.0	25.0	100.0	40.6	100.0	25.0	79.5	25.0	61.0	25.0	66.0	47.2	38.2	26.2	46.5
2	100.0	30.3	100.0	25.0	100.0	44.6	100.0	25.0	86.0	25.0	64.2	25.0	70.9	50.5	41.8	27.5	51.5
3	100.0	28.4	100.0	25.0	100.0	40.9	100.0	25.0	79.9	25.0	61.2	25.0	66.2	47.4	38.5	26.0	46.8
4	100.0	17.0	100.0	9.0	100.0	53.5	100.0	9.0	89.5	9.0	53.5	9.0	67.1	48.0	50.7	14.2	59.4
5	100.0	28.4	100.0	25.0	100.0	39.5	100.0	25.0	76.5	25.0	59.0	25.0	62.6	44.1	38.5	26.1	44.3
6	100.0	33.0	100.0	25.0	100.0	49.5	100.0	25.0	92.9	25.0	67.3	25.0	73.7	52.3	48.1	29.7	56.4

The obtained designs do not include any local constrains on stress and local buckling. Nevertheless, the designs do not exceed an admissible stress of σ_{adm} = 344.7 MPa from (Aydoğdu et al., 2023) even taking the corrosion reduction into consideration. Still, local member buckling is observed in the designs for members 3, 7, 8 and 11, which is the weakness of the proposed approach.

[3]CVX considers the high level of the requested solver accuracy at $\epsilon^{3/4}$, where machine double precision constant assumed $\epsilon = 2.2 \times 10^{-16}$. Low and medium precisions use tolerances $\epsilon^{3/8}$ and $\epsilon^{1/2}$, respectively.

Tab. 4: Summary over the obtained design problem in Example 1 obtained with SeDuMi solver. The reference mass of structure without corrosion effect is $m_{\text{ref}} = 1878.4$ kg for cases 1, 2 and 3, $m_{\text{ref}} = 1788.4$ kg for case 4 and $m_{\text{ref}} = 1935.7$ kg for case 6. All values are rounded to 0.1 cm^2.

case	m_{tot}, kg	m_{corr}, kg	β, %	iterations	CPU time, s
0	1878.4	-	-	17	0.09
1	1971.3	92.8	4.9	17	0.17
2	2049.6	171.1	9.1	17	0.17
3	1974.2	95.7	5.1	146	0.65
4	1885.8	97.4	5.4	146	0.86
5	1935.7	-	-	15	0.26
6	2135.7	197.7	10.2	17	0.32

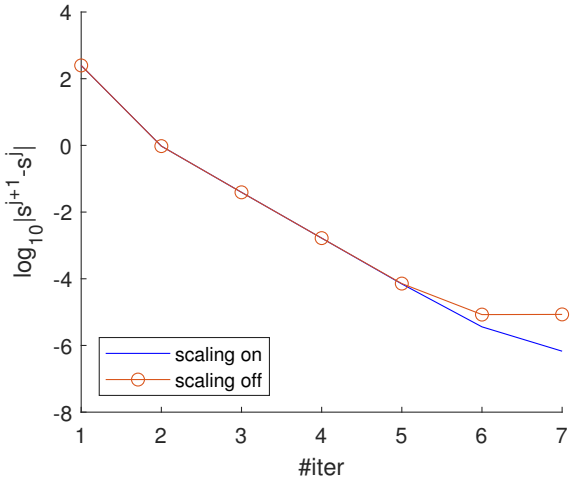

Fig. 7: Convergence $\log |\mathbf{s}^{j+1} - \mathbf{s}^{j}|$ of the norm over convex-concave iterations for Example 1, case 4, SDPT3 solver.

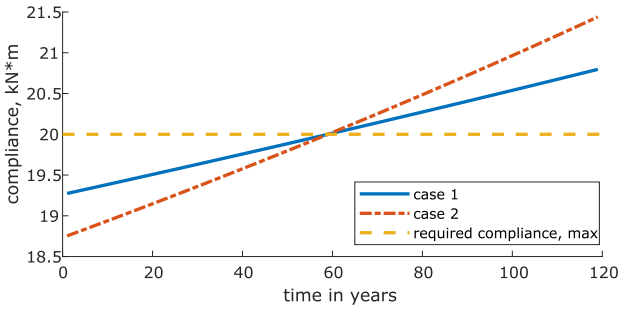

Fig. 8: Degradation of the compliance over time for optimal designs in Example 1 for cases 1 and 2.

4.2 Example 2: 33-member truss

Consider a 2D grid structure with 33 members[4] shown in Figure 9 (left). The structure is fixed at the three utmost left nodes and is loaded at the centre node of the right row with a vertical force $F = 80$ kN. The self-weight is neglected. The admissible compliance is selected $\bar{\tau} = 150$ N·m. Material parameters correspond to a regular steel: $E = 210$ GPa, $\rho = 7800$, kg/m^3, $a = -0.120 \cdot 10^{-4}$ cm/year/$^\circ$ and $b = 20.0 \cdot 10^{-4}$ cm/year. Varied parameters for four cases are presented in Table (5). In case 1, we seek for the optimal design for the FW problem for different required lifespan up to 240 years. The extended required lifespan compared to previous example can illustrate two features. First, a super-linear growth of the added mass vs. required lifespan. Second, the optimization problems can become infeasible for a critical lifespan of the structure. In cases 2, 3 and 4, we seek for the optimal design for the FAR problem with 3 different aspect ratios, but a fixed required lifespan of 60 years. Furthermore, the designs using weighting (24) and (25) are compared using relative weighted norm $\epsilon = |\mathbf{s}^* - \tilde{\mathbf{s}}^*|/|\mathbf{s}^*|$.
The optimized design for the FW problem and required life 60 years is shown in Figure 9 (middle). Trusses at the lower and upper belts as well as one X-bracing are assigned the largest admissible cross-sections. Figure 9 (right) gives the total mass correction for the range of required service life years. The correction grows faster than linear with no feasible design possible for required life above 250 years[5]. The added mass for the required life 240 years reaches 114.64% due to corrosion depth in range of 0.325 cm to 0.375 cm for different orientations and it cannot be neglected in design.

[4] A similar grid structure was used for a different optimization problem in (Tkachuk and Tkachuk, 2024)

[5] SDPT3 and SeDuMi solvers suspect the problem being infeasible. Furthermore, the design with all $h_e = \bar{h}$ gives possible compliance $\tau \approx 0.603$ kN·m, which is above the limit $\bar{\tau} = 0.6$ kN·m, i.e., even with strongest sections the structure does not fulfil requirements after corrosion reduction.

Tab. 5: Parameters for the design problem in Example 2.

case	Attr.	t, year	w, cm	$\bar{h}$, cm	$\underline{h}$, cm	α	$\bar{A}$, cm^2	$\underline{A}$, cm^2
1	FW	≤ 240	2	8	2	-	-	-
2	FAR	60	-	-	-	0.5	16	4
3	FAR	60	-	-	-	1.0	16	4
4	FAR	60	-	-	-	2.0	16	4

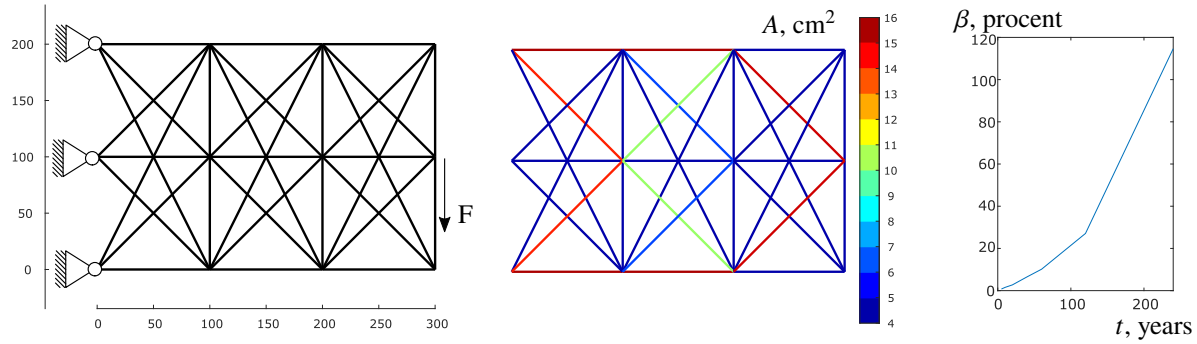

Fig. 9: Setup of Example 2 with all sizes are in cm (left), obtained design for required lifespan of 60 years (middle) and required relative added mass (right).

In cases 2, 3 and 4, the general layout of the solution is similar to one obtained for case 1 ($t = 60$ years) shown in Figure 9, middle. The summary for cases 2, 3 and 4 are presented in Table 6. A relative increase in mass between 9.99% and 10.4% is required. Aspect ratios above one are marginally more efficient. No significant difference between results using (7) and (8) is observed.

Tab. 6: Summary of results for cases 2, 3 and 4 of Example 2. The reference mass of structure without corrosion effect $m_{\text{ref}} = 223.2$ kg.

Aspect ratio α, -	0.5	1.0	2.0
Added mass m_{corr}, kg	23.2	22.7	22.3
Increase, β, %	10.4	10.2	9.99
Difference in the solution using (24) and (25), ϵ	$1.22 \cdot 10^{-5}$	$9.35 \cdot 10^{-6}$	$1.14 \cdot 10^{-5}$

4.3 Example 3: 3660-member truss grid with fixed width of cross-sections and elliptical uncertainty in load

The final example considers a truss grid with 30×30 cells shown in Figure 10 (left). Each cell has a dimension of 0.6×0.6 m and is stiffened by a pair of diagonal members that are not connected at the intersection. The topology and load for the structure do not have a direct application, but the setup can be easily scaled to see the computational limit of the approach. Material parameters correspond to a regular steel identical to Example 2: $E = 210$ GPa, $\rho = 7800$, kg/m^3, $a = -0.120 \cdot 10^{-4}$ cm/year/° and $b = 20.0 \cdot 10^{-4}$ cm/year. The width of all rectangular cross-sections $w = 2$ cm, while the limits on the height $\bar{h} = 8$ cm and $\underline{h} = 2$ cm. These cross-section dimensions are similar to values presented in Example 1. The structure is supported in the vertical direction at the lowest layer of nodes and in the horizontal direction at two nodes at the left row: the left bottom corner and the 6th node from the bottom. An elliptical uncertainty for the load is assumed with three load vectors ($k = 3$). Load case 1 is a pair of downward forces $F = 150$ kN at the top right and left corners. Load case 2 is a pair of horizontal forces $F = 70$ kN at the top right and left corners. Load case 3 distributes a horizontal force total of $F = 120$ kN at the top row of nodes. The self-weight is neglected. The admissible compliance is selected $\bar{\tau} = 0.6$ kN·m. We seek an optimal design for the structure for a required life of 60 years. For this size of the problem, only the SDP solver from MOSEK produces the best results and it is used herein. It is twice faster and uses half of interior point iterations compared to SeDuMi. SeDuMi requires 89 interior point iterations, which is beyond the limit of 80. Solver SDPT3 does not converges at all (it suspects the problem being infeasible).

The design is obtained in 486 s of runtime and 37 interior point iterations for high precision settings (357 s and 35 iterations for medium precision). The distribution of optimal areas is in Figure 11. The majority of members (2661) have an area close to the bottom limit of 4 cm^2. 335 members have area at the upper limit (16 cm^2) and they concentrate along three major load paths, shown in Figure 10 (right). 664 members have intermediate values of the cross-sections. Noteworthy, the difference in the total mass between MOSEK and SeDuMi is below 0.07 %.

The total mass of the structure $m_{\text{tot}} = 11.865$ ton, which corresponds to a correction of $\beta = 10.9\%$ ($m_{\text{ref}} = 10.871$ ton). The design without corrosion correction has 2661 members with an area close to the bottom limit 4 cm^2 and only 335 members with an area at the upper limit (16 cm^2). The observed correction of $\beta = 10.9\%$ is larger than the reduction of the thickest section 2×8 cm^2 (ca. 7.2%). This aligns with the observation that the most efficient members for minimizing compliance are those at the upper bound of the admissible area, while neighbouring members tend to be less efficient.

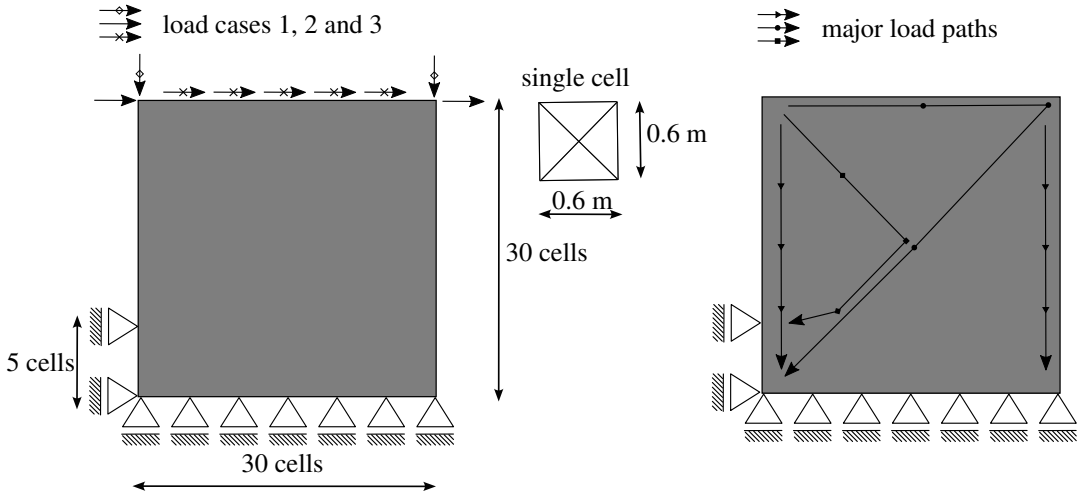

Fig. 10: Setup of Example 3 (left) and major load paths (right).

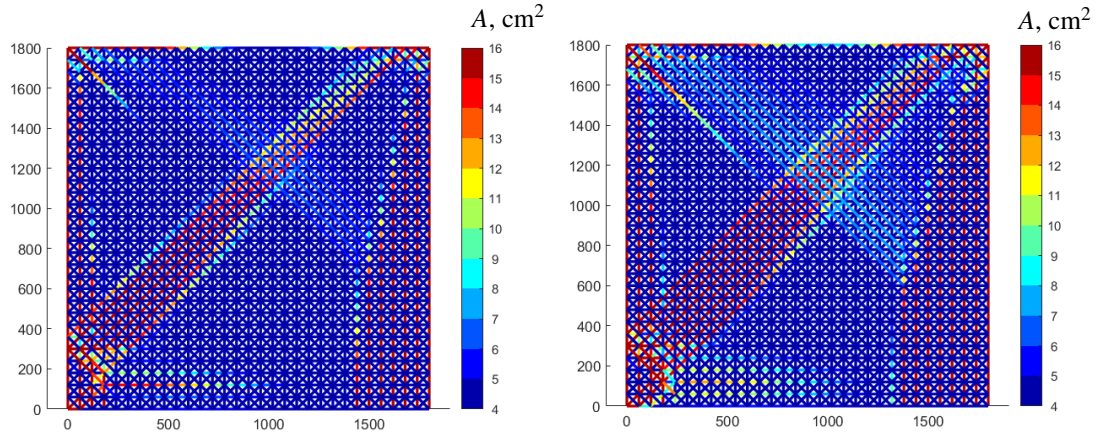

Fig. 11: Obtained designs for Example 3 without a corrosion correction (left) and with a corrosion correction (right). All dimensions in cm.

The two worst combinations of loads for the optimized design with equal compliance values $\tau = 0.6$ kN·m are

$$\zeta^{(1)} = \begin{bmatrix} 0.9983 & 0.0447 & -0.0384 \end{bmatrix}, \tag{35}$$

$$\zeta^{(2)} = \begin{bmatrix} -0.0589 & 0.7785 & 0.6273 \end{bmatrix}. \tag{36}$$

The first worst load is dominated by the vertical load (load case 1). The second worst load combines two horizontal load cases (2 and 3).
The obtained designes are also checked for local stress and buckling constraints. Only five combinations of loads are used for the purpose: load cases 1, 2 and 3 separately and two worst scenarios in (35) and (36). The maximum observed stress is 68.7 MPa, which is below the yield strength of most of structural steels. The local buckling stress is never reached (the worst load scenario 2 gives the least local buckling safety factor of 2.42).

5 Conclusion

The proposed corrosion correction approach for the sizing of truss structures under global compliance constraints is shown to work for rectangular sections with fixed width and fixed aspect ratio. It relies on a uniform corrosion model of cross-sections leading to reduction of effective area depending on the exposure time and orientation of the truss members. The sizing problem can be formulated as a continuous optimization problem on a convex set defined by the limits on the cross-sections and a given compliance of the structure. Both, a single load and elliptical uncertainty of the load can be included in the compliance constraint via the Schur complement. A combination of an active load and self-weight is also considered. Any infeasible design is identified as an empty set, e.g., when the structure with the maximum allowed cross-sections fails the compliance constraint due to corrosion reduction (typically at a large required life of the structure). Two cases of the cross-section are considered in detail. The fixed width case leads to a convex objective. The fixed aspect ratio case leads to an objective with a dominating convex term and a minor concave term, which is treated iteratively with a standard convex-concave procedure. An exact and approximate mapping of the effective area on the initial area gives nearly identical results for the optimization. Fixed aspect ratio case increases the computational cost approximately by a factor of seven due to an outer loop in the convex-concave procedure. Both cases fit well

with existing SDP frameworks and can be solved using CVX.
SDP solvers SDPT3 and SeDuMi work equally well for small problems, while large problems need to rely on MOSEK for efficiency and robustness reasons. Proper scaling of the objective and constraints helps the convergence of the SDP solvers. The typical iteration numbers range from 17 to 43.
The added mass due to corrosion correction is similar to the reduction of the effective cross-sections in cases where the truss members can be made thicker along the most efficient load paths. Otherwise, the added mass is spread between truss members along less efficient load paths, leading to a higher added total mass.
The current formulation disregards stress or buckling constraints, which is the most significant limitation. Thus, no direct comparison with Aydoğdu et al. (2023) is possible even for a simple 17-member example. Local buckling constraints would make the design more sensitive to the aspect ratio than observed in the presented examples, which is a limitation of the proposed approach. Still, the obtained results can be used for benchmarking purposes and inspire further method development.
Only cross-sections with a single design parameter that directly maps to both area and perimeter can be included. An extension to square hollow sections is discussed in A.1 if a power scaling between the width and the wall thickness is assumed. Furthermore, accurate data for corrosion of circular and square hollow sections is scarce. Future work can address both limitations.
Minor extensions for the future include the formulation for 3D trusses, adding constraints on the base frequency and grouping members to have the same section. Furthermore, the dual problem for minimizing the compliance at given lifespan for a given initial volume of a truss structure can be formulated and solved. The major extensions include frames, adding intermediate repair and a correction due to a corrosion at the connection of the members.

Acknowledgments

This research did not receive any specific grant from funding agencies in the public, commercial, or non-for-profit sectors. Fast prototyping of the proposed methods would not be possible without free access to CVX package and solvers SDPT3, SeDuMi and MOSEK, which is gratefully acknowledged. Authors also acknowledge kind invitation to present the early version of the paper at seminars hosted by Prof. M. Bischoff at University of Stuttgart and Prof. M. Stingl at Friedrich-Alexander-Universität Erlangen-Nürnberg. Useful comments from these seminar talks improved the manuscript. Furthermore, comments from anonymous reviewers helped to improve the manuscript.

Data and code availability

Code is uploaded to a public GitHub project https://github.com/DrTkachuk/CorrosionCorrectedTrussOptimization/tree/main.

Appendix

A.1 Potential design variables for thin-walled box sections

Structural hollow sections with anti-corrosive properties provide a good alternative to content presented in the previous sections due to minimized maintenance and higher buckling stress in compression. For a square hollow section, two main dimensions are the wall thickness w and the height h. Steel mills produce multiple wall thickness dimensions for the same height (usually 4 or 5). It is not possible to select one design parameter defining the nominal cross-sectional area A and the perimeter exposed to corrosion, contrary to to solid sections in the main body of the article. In order to map the area and perimeter to a single continuous variable, two steps are required. First, the variety is reduced to a subfamily, e.g., light or heavy. Approximating intermediate values of area via interpolation.
A linear regression in log space for square hollow sections from (SSAB Weathering Tube 355WH) predicts a power scaling of area and wall thickness with height as

$$A = 4wh \sim h^{\gamma}, \qquad w \sim h^{\gamma-1}, \qquad \gamma_{\text{light}} \approx 1.677, \qquad \gamma_{\text{heavy}} \approx 1.897. \tag{A.1}$$

Figure A.1 illustrates the quality of the fit. Thus, the effective cross-section area can be expressed as a function of time and the initial area as

$$A_r = A^{\frac{1}{\gamma}}\left(A^{\frac{\gamma-1}{\gamma}} - \tilde{c}_1 t\right) + \tilde{c}_2 t^2, \tag{A.2}$$

where constants $\tilde{c}_1$ and $\tilde{c}_2$ depend on the corrosion model (on the outside perimeter) and the orientation of the member. Exact corrosion data is not available for these sections, which is a first obstacle for further studies. Inverting this function for the objective is not practical. Instead, the Taylor expansion around $(t = 0, A_r = A)$ is possible using the implicit function theorem. The expression up to the second term yields

$$A = A_r + A_r^{\frac{1}{\gamma}}\tilde{c}_1 t + \left(\frac{1}{\gamma} A_r^{\frac{\gamma-2}{\gamma}}\tilde{c}_1^2 - \tilde{c}_2\right) t^2 + O(t^3). \tag{A.3}$$

The latter expression has a dominant linear (convex) term A_r and two minor concave terms, which fits the concave-convex procedure for regular values $1 < \gamma < 2$ (case $\gamma = 2$ is recovered for the fixed aspect ratio solid square sections). Nevertheless, these sections are not considered in the examples and formulations.

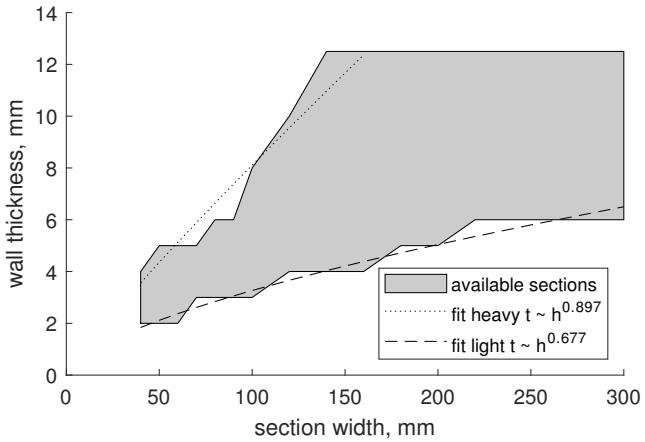

Fig. A.1: Dimensions of square hollow sections in 355WH steel from (SSAB Weathering Tube 355WH).

References

Wolfgang Achtziger and Martin P Bendsøe. Optimal topology design of discrete structures resisting degradation effects. *Structural Optimization*, 17(1):74–78, 1999.

Wolfgang Achtziger and Michal Kočvara. On the maximization of the fundamental eigenvalue in topology optimization. *Structural and Multidisciplinary Optimization*, 34(3):181–195, 2007.

Afranur Yaren Aydoğdu, Musa Artar, and Mustafa Ergün. Optimum weight design of steel truss roof systems considering corrosion effect. *Structures*, 49:88–105, 2023.

Atorod Azizinamini, Edward H Power, Glenn F Myers, H Celik Ozyildirim, Eric S Kline, David W Whitmore, and Dennis R Mertz. Design guide for bridges for service life. Technical report, 2014.

Bence Balogh, Matteo Bruggi, and Janos Lógó. Optimal design accounting for uncertainty in loading amplitudes: A numerical investigation. *Mechanics Based Design of Structures and Machines*, 46(5):552–566, 2018.

Aharon Ben-Tal and Arkadi Nemirovski. Robust truss topology design via semidefinite programming. *SIAM journal on optimization*, 7(4):991–1016, 1997.

British Standards Institution. Eurocode - basis of structural design. Standard BS EN 1990:2002+A1:2005, British Standards Institution, London, 2005. Incorporating corrigenda December 2008 and April 2010.

ASL Chan. The design of michell optimum structures. *Aeronautical Research, Council Reports and Memoranda*, 3303:1–40, 1960.

Anikó Csébfalvi and János Lógó. Investigation of the possible numerical treatments of a compliance-function-shape-oriented robust truss sizing model with uncertain loading directions. *Advances in Engineering Software*, 149:102899, 2020.

Maryam Fazel, Haitham Hindi, and Stephen P Boyd. Log-det heuristic for matrix rank minimization with applications to hankel and euclidean distance matrices. In *Proceedings of the 2003 American Control Conference*, volume 3, pages 2156–2162. IEEE, 2003.

C Fleury. A unified approach to structural weight minimization. *Computer Methods in Applied Mechanics and Engineering*, 20(1): 17–38, 1979.

Herbert Martins Gomes. Truss optimization with dynamic constraints using a particle swarm algorithm. *Expert Systems with Applications*, 38(1):957–968, 2011.

Michael Grant and Stephen Boyd. *CVX users' guide, Release 2.2*. CVX Research, Inc., 2020.

Michael C Grant and Stephen P Boyd. Graph implementations for nonsmooth convex programs. In *Recent advances in learning and control*, pages 95–110. Springer, 2008.

Soodeh Habibi. *Algorithms and Software for Structured Semidefinite Optimization*. PhD thesis, University of Birmingham, 2024.

Soodeh Habibi, Arefeh Kavand, Michal Kočvara, and Michael Stingl. Barrier and penalty methods for low-rank semidefinite programming with application to truss topology design. *arXiv preprint arXiv:2105.08529*, 2021.

Soodeh Habibi, Michal Kočvara, and Michael Stingl. Loraine–an interior-point solver for low-rank semidefinite programming. *Optimization Methods and Software*, pages 1–31, 2023.

Daiki Hashimoto and Yoshihiro Kanno. A semidefinite programming approach to robust truss topology optimization under uncertainty in locations of nodes. *Structural and Multidisciplinary Optimization*, 51:439–461, 2015.

ISO 9223:2012. Corrosion of Metals and Alloys – Corrosivity of Atmospheres – Classification, Determination, and Estimation. Standard, International Organization for Standardization, Geneva, CH, 2012.

Rachel H. Jordan, editor. *Structural stability condition assessment of corroded steel trusses in operating industrial facilities*, St. Louis, Missouri, April 2-5, 2019, 2019. Structural Stability Research Council (SSRC).

Shigenobu Kainuma, Muye Yang, Yang Gao, and Mikio Hashimoto. Long-term deterioration mechanism of hot-dip aluminum coating exposed to a coastal-atmospheric environment. *Construction and Building Materials*, 280:122516, 2021.

Yoshihiro Kanno. *Nonsmooth mechanics and convex optimization*. Crc Press Boca Raton, 2011.

Yoshihiro Kanno. Global optimization of trusses with constraints on number of different cross-sections: a mixed-integer second-order cone programming approach. *Computational Optimization and Applications*, 63:203–236, 2016.

Yoshihiro Kanno. Redundancy optimization of finite-dimensional structures: Concept and derivative-free algorithm. *Journal of Structural Engineering*, 143(1):04016151, 2017.

Meryem Keleş, Musa Artar, and Mustafa Ergün. Investigation of temperature effect on the optimal weight design of steel truss bridges using cuckoo search algorithm. *Structures*, 59:105819, 2024.

NS Khot. Optimization of structures with multiple frequency constraints. *Computers & Structures*, 20(5):869–876, 1985.

D. Knotkova-Cermakova, J. Vlckova, and J. Honzak. Atmospheric corrosion of weathering steels. In *Atmospheric Corrosion of Metals*, pages 7–44. ASTM, 1982.

Michal Kočvara. On the modelling and solving of the truss design problem with global stability constraints. *Structural and multidisciplinary optimization*, 23:189–203, 2002.

Michal Kočvara and Jirı V Outrata. Inverse truss design as a conic mathematical program with equilibrium constraints. *Discrete Contin. Dyn. Syst. Ser. S*, 10:1329–1350, 2017.

Wies law Kowalski, Mateusz Richter, and Katarzyna Tokarczyk. Effect of icing as a non-structural mass on the variation of natural frequency of a lightweight lattice structure. *Archives of Civil Engineering*, pages 37–53, 2023.

Raffaele Landolfo, Lucrezia Cascini, and Francesco Portioli. Sustainability of steel structures: Towards an integrated approach to life-time engineering design. *Frontiers of Architecture and Civil Engineering in China*, 5(3):304–314, 2011.

C Leygraf. Atmospheric corrosion. *A John Wiley and Sons*, 32, 2000.

Wei Lingyun, Zhao Mei, Wu Guangming, and Meng Guang. Truss optimization on shape and sizing with frequency constraints based on genetic algorithm. *Computational Mechanics*, 35(5):361–368, 2005.

Thomas Lipp and Stephen Boyd. Variations and extension of the convex–concave procedure. *Optimization and Engineering*, 17: 263–287, 2016.

János Lógó, Hussein Ismail, et al. Milestones in the 150-year history of topology optimization: A review. *Computer Assisted Methods in Engineering and Science*, 27(2-3):97–132, 2020.

Shenyuan Ma, Jakub Mareček, Vyacheslav Kungurtsev, and Marek Tyburec. Truss topology design under harmonic loads: peak power minimization with semidefinite programming. *Structural and Multidisciplinary Optimization*, 68(2):40, 2025.

Thomas L Magnanti and Dan Stratila. Separable concave optimization approximately equals piecewise-linear optimization. *arXiv preprint arXiv:1201.3148*, 2012.

Anthony George Maldon Michell. The limits of economy of material in frame-structures. *Philosophical Magazine and Journal of Science*, 8(47):589–597, 1904.

MOSEK ApS. Mosek modeling cookbook, 2022. URL https://docs.mosek.com/modeling-cookbook/index.html.

M Ohsaki, K Fujisawa, N Katoh, and Y Kanno. Semi-definite programming for topology optimization of trusses under multiple eigenvalue constraints. *Computer Methods in Applied Mechanics and Engineering*, 180(1-2):203–217, 1999.

Alessio Pipinato. Extending the lifetime of steel truss bridges by cost-efficient strengthening interventions. *Structure and Infrastructure Engineering*, 14(12):1611–1627, 2018.

William Prager. Optimal layout of cantilever trusses. *Journal of Optimization Theory and Applications*, 23:111–117, 1977.

SD Rajan. Sizing, shape, and topology design optimization of trusses using genetic algorithm. *Journal of Structural Engineering*, 121(10):1480–1487, 1995.

Zabihullah Rasoli, Kazutoshi Nagata, Takeshi Kitahara, and Kunitomo Sugiura. Improvement of accuracy for the evaluation of corrosion environment on steel bridges using wrf technique. *Journal of Structural Engineering, A*, 66:452–465, 2020.

Javier E Rodríguez-Yáñez, Sebastián Feliu Batlle, Jean Sanabria-Chinchilla, and José Félix Rojas-Marín. Combined effect of the exposure angle and face orientation on the atmospheric corrosion behavior of low carbon steel. *Electrochimica Acta*, 439: 141567, 2023.

Juan J Santana, Víctor Cano, Helena C Vasconcelos, and Ricardo M Souto. The influence of test-panel orientation and exposure angle on the corrosion rate of carbon steel. mathematical modelling. *Metals*, 10(2):196, 2020.

Richard T Shield. Optimum design of structures through variational principles. In *Optimization and Stability Problems in Continuum Mechanics*, pages 13–37. Springer, 1971.

Qianjin Shu, Kejin Wang, Guanglin Yuan, Yunfei Zhang, Limin Lu, and Ziyuan Liu. Assessing capacity of corroded angle members in steel structures based on experiment and simulation. *Construction and Building Materials*, 244:118210, 2020.

SSAB Weathering Tube 355WH. Data sheet SSAB Weathering Tube 355WH circular, rectangular, square and special shapes.

Mathias Stolpe. Truss optimization with discrete design variables: a critical review. *Structural and Multidisciplinary Optimization*, 53:349–374, 2016.

Mathias Stolpe. Fail-safe truss topology optimization. *Structural and Multidisciplinary Optimization*, 60(4):1605–1618, 2019.

Jos F Sturm. Using SeDuMi 1.02, a MATLAB toolbox for optimization over symmetric cones. *Optimization Methods and Software*, 11(1-4):625–653, 1999.

Krister Svanberg. Optimization of geometry in truss design. *Computer Methods in Applied Mechanics and Engineering*, 28(1): 63–80, 1981.

Anton Tkachuk and Mykola M Tkachuk. Design of truss structures with multiple eigenfrequency constraints via rank minimization. *Computers & Structures*, 299:107392, 2024.

Konstantinos Daniel Tsavdaridis, Andreas Nicolaou, Anand Dipak Mistry, and Evangelos Efthymiou. Topology optimisation of lattice telecommunication tower and performance-based design considering wind and ice loads. *Structures*, 27:2379–2399, 2020.

Reha H Tütüncü, Kim-Chuan Toh, and Michael J Todd. Solving semidefinite-quadratic-linear programs using SDPT3. *Mathematical Programming*, 95:189–217, 2003.

Georgios Tzortzinis, Brendan T Knickle, Alexander Bardow, Sergio F Breña, and Simos Gerasimidis. Strength evaluation of deteriorated girder ends. i: Experimental study on naturally corroded i-beams. *Thin-Walled Structures*, 159:107220, 2021.

R Vera, BM Rosales, and C Tapia. Effect of the exposure angle in the corrosion rate of plain carbon steel in a marine atmosphere. *Corrosion Science*, 45(2):321–337, 2003.

Renhua Wang, R Ajit Shenoi, and Adam Sobey. Ultimate strength assessment of plated steel structures with random pitting corrosion damage. *Journal of Constructional Steel Research*, 143:331–342, 2018.

Kazuo Yonekura and Yoshihiro Kanno. Global optimization of robust truss topology via mixed integer semidefinite programming. *Optimization and Engineering*, 11:355–379, 2010.